









SHORT COMMUNICATION

A suitable strategy to find IAA metabolism mutants

Rubén Casanova-Sáez¹  | Aleš Pěnčík^{1,2}  | Rafael Muñoz-Viana¹  |
 Federica Brunoni¹  | Rui Pinto³  | Ondřej Novák²  | Karin Ljung¹  |
 Eduardo Mateo-Bonmatí^{1,4} 

¹Umeå Plant Science Centre (UPSC), Department of Forest Genetics and Plant Physiology, Swedish University of Agricultural Sciences, Umeå, Sweden

²Laboratory of Growth Regulators, Institute of Experimental Botany, The Czech Academy of Sciences & Faculty of Science, Palacký University, Olomouc, Czech Republic

³Computational Life Science Cluster (CLiC), Chemistry department (KBC), Umeå University, Umeå, Sweden

⁴Centro de Biotecnología y Genómica de Plantas, Universidad Politécnica de Madrid (UPM), Instituto Nacional de Investigación y Tecnología Agraria y Alimentaria (INIA)/CSIC, Pozuelo de Alarcón, Madrid, Spain

Correspondence

Karin Ljung

Email: karin.ljung@slu.se

Eduardo Mateo-Bonmatí

Email: eduardo.mateo@upm.es

Present addresses

Rubén Casanova-Sáez, Umeå Plant Science Centre (UPSC), Department of Plant Physiology, Umeå University, Umeå, Sweden;
 Rafael Muñoz-Viana, Unidad de Bioinformática, Instituto de Investigación Sanitaria Puerta de Hierro-Segovia de Arana, Majadahonda, Spain;
 Federica Brunoni, Laboratory of Growth Regulators, Institute of Experimental Botany, The Czech Academy of Sciences & Faculty of Science, Palacký University, Olomouc, Czech Republic; and Rui Pinto, Department of Epidemiology and Biostatistics, School of Public Health, Imperial College, London, UK.

Funding information

The Knut and Alice Wallenberg Foundation, Grant/Award Number: KAW 2016.0352; Carl Tryggers foundation, Grant/Award Numbers: CTS 12:289, CTS 13:275; Vetenskapsrådet, Grant/Award Number: 2014-04514; Kempestiftelserna, Grant/Award Numbers: JCK-1111, JCK-1811; Agencia Estatal de Investigación, Grant/Award Numbers: PID2023-147737NA-I00, RYC2021-030895-I; Palacký University Olomouc, Grant/Award Number: IGA_PrF_2024_013

Edited by S. Robert

Abstract

Indole-3-acetic acid (IAA), the most common form of auxin, is involved in a great range of plant physiological processes. IAA is synthesized from the amino acid tryptophan and can be transported and inactivated in a myriad of ways. Despite intense research efforts, there are still dark corners in our comprehension of IAA metabolism and its interplays with other pathways. Genetic screens are a powerful tool for unbiasedly looking for new players in a given biological process. However, pleiotropism of auxin-related phenotypes and indirect effects make it necessary to incorporate additional screening steps to specifically find mutants affected in IAA homeostasis. We previously developed and validated a high-throughput methodology to simultaneously quantify IAA, key precursors, and inactive forms from as little as 10 mg of fresh tissue. We have carried out a genetic screening to identify mutants involved in IAA metabolism. Auxin reporters *DR5_{pro}:VENUS* and *35S_{pro}:DII-VENUS* were EMS-mutagenized and subjected to a parallel morphological and reporter-signal pre-screen. We then obtained the auxin metabolite profile of 325 M₃ selected lines and used multivariate data analysis to identify potential IAA-metabolism mutants. To test the screening design, we identified the causal mutations in three of the candidate lines by mapping-by-sequencing: *dii365.3*, *dii571.1* and *dr693*. These carry new alleles of *CYP83A1*, *MIAO*, and *SUPERROOT2*, respectively, all of which have been previously involved in auxin homeostasis. Our results support the suitability of this approach to find new genes involved in IAA metabolism.

Rubén Casanova-Sáez and Aleš Pěnčík contributed equally to this work. Karin Ljung and Eduardo Mateo-Bonmatí contributed equally to this work.

This is an open access article under the terms of the [Creative Commons Attribution-NonCommercial-NoDerivs](https://creativecommons.org/licenses/by-nc-nd/4.0/) License, which permits use and distribution in any medium, provided the original work is properly cited, the use is non-commercial and no modifications or adaptations are made.

© 2025 The Author(s). *Physiologia Plantarum* published by John Wiley & Sons Ltd on behalf of Scandinavian Plant Physiology Society.

1 | INTRODUCTION

From the embryo to the flower, auxin is a key player in many plant developmental processes (Casanova-Sáez and Voß 2019, Casanova-Sáez et al. 2021). It is also crucial for the integration of environmental signals by driving tropisms (phototropism, gravitropism, hydrotropism, halotropism, or thigmotropism), and the response to abiotic and biotic stresses (Kazan and Manners 2009, Jing et al. 2023). The cellular response to auxin relies on its concentration, which results from local biosynthesis, polar transport and inactivation. Far from linearity, IAA, the most common auxin form, is synthesized by the action of several parallel pathways with known intermediates such as indole-3-acetaldoxime (IAOx), indole-3-acetonitrile (IAN), and indole-3-pyruvic acid (IPyA) (Casanova-Sáez et al. 2021). IAA concentration is also controlled by inactivation and degradation. Indeed, most of the IAA present in the cell is inactive, either as a storage form (forms that can be reverted to active IAA) or as IAA catabolites (irreversibly inactive) (Casanova-Sáez et al. 2021). The main storage forms are the ester-linked IAA-glucose (IAA-glc) and amide-linked IAA, encompassing a group of compounds including IAA conjugates to amino acids (IAA-aa) and small peptides. Most abundant IAA catabolites are the oxidized form 2-oxindole-3-acetic acid (oxIAA), its glycosylated counterpart oxIAA-glc and two amide-linked IAA conjugates, IAA-Asp and IAA-Glu.

To further understand all the interconnected pathways around IAA homeostasis and their connections with other metabolic routes, we previously developed a liquid-chromatography coupled to mass-spectrometry LC-MS/MS method to quantify the levels of IAA and ten IAA-related metabolites simultaneously: the precursors anthranilate (Ant), and Trp; the intermediate forms IAOx, IAN, and IPyA; and the inactive forms oxIAA, IAA-glc, oxIAA-glc, IAA-Asp, and IAA-Glu. Starting with just about 10 mg of fresh tissue and separation times faster than four minutes, this method proved to be a high-throughput approach able to deal with a high number of samples in a relatively short time (Pěnčík et al. 2018).

Aiming to discover new genes and connections among known pathways involved in IAA homeostasis, we now have applied our high-throughput IAA metabolite profiling method as a filtering step through a forward genetic screen. We first chemically mutagenized two popular auxin reporters, *DR5_{pro}:VENUS* and *35S_{pro}:DII-VENUS*, and preselected a cohort of 325 M₃ lines showing aberrant reporter signals and/or morphological traits. We then measured the IAA metabolome among the mutant lines and used multivariate data analysis and mapping-by-sequencing to select candidates and identify the causal mutations. Our results proved that this is a suitable approach to search for players in IAA metabolism and homeostasis.

2 | MATERIALS AND METHODS

2.1 | Plant material and growth conditions

Seeds from the *Arabidopsis thaliana* (L.) Heynh. SALK_123405 (N623405), GT_5_15667 (N175555), GABI_789A10 (N737119),

WiscDsLoxHs180_01G (N917191) were obtained from the Nottingham Arabidopsis Stock Centre. The presence and position of all insertions were confirmed by PCR amplifications using gene-specific primers together with the insertion-specific primers LBb1.3 (for the SALK line), Ds3_1 (for the GT line), LB-PAC161 (for the GABI line), and LB-WiscDsLoxHs (for the Wisc line). All the primers are listed in the Table S1. The reporter lines *35S_{pro}:DII-VENUS* (Col-0 background) (Brunoud et al. 2012) and *DR5_{pro}:VENUS* (Ler background) (Heisler et al. 2005), and the *sur2-1* mutant (Ws background) (Barlier et al. 2000) were previously described.

Arabidopsis seeds were surface-sterilized with 40% v/v commercial bleach and 0.002% Triton-X-100 for 10 minutes and then washed four times with sterile deionized water. Seeds were stratified for a minimum of 2 days and then sowed under sterile conditions on square Petri dishes containing half-strength Murashige & Skoog salt mixture (M0221; Duchefa Biocemie), 0.05% MES hydrate (M2933; Sigma), and 0.8% plant agar (P1001; Duchefa Biochemie) with the pH adjusted to 5.7 with potassium hydroxide. Plants were kept in vitro for a maximum of 2 weeks, after which they were transferred to pots containing a 3:1 mixture of organic soil and vermiculite. All plants were grown under long-day conditions (16 h:8 h, light:dark) at 22 ± 1°C and cool white fluorescent light (150 μmol photons m⁻² s⁻¹).

2.2 | EMS mutagenesis

For the EMS mutagenesis, we followed the standardized procedure from Ottoline Leyser and Ian J. Funder (University of Cambridge, UK), deposited in the TAIR website (https://www.arabidopsis.org/download/file?path=Protocols%2Fcomplete_guide%2F6_EMS_mutagenesis.pdf).

Briefly, we mutagenize 100 mg (≈5,000 seeds) of healthy seeds from each parental line, by soaking them for 4 hours in a solution containing 100 mM sodium phosphate, pH 5, 5% DMSO, and 100 mM of EMS. We then washed the seeds twice with 100 mM sodium thiosulfate for 15 minutes and then twice with water for 15 minutes. In total, we recovered 2230 M₂ (1284 from *35S_{pro}:DII-VENUS* and 946 from *DR5_{pro}:VENUS* background) families from selfing M₁ individual plants. To screen the M₂ families, mutagenized seeds, Col-0, and the corresponding parental line were sown in four rows per plate, with about 30 seeds per row, to inspect the VENUS signal and morphological phenotypes. Mutant lines were named in the format *diixxx.x* or *drxxx.x*, where *dii* and *dr* indicate lines in *35S_{pro}:DII-VENUS* or *DR5_{pro}:VENUS* background, respectively. The following number corresponds to the M₂ family number. An additional number after a dot was used when a different phenotype, or a phenotype of different intensity, was observed in the segregation of a given M₂ family.

2.3 | Light and confocal microscopy

Seedlings were imaged in a stereomicroscope MZ9.5 (Leica) equipped with CCD camera MC190HD. The VENUS signal in 5-day-old M₂ seedling roots was rapidly screened by placing whole agar plates

under a Macroconfocal LSI HSC (Leica). The VENUS signal in 7-day-old seedling roots from candidate lines was imaged in an LSM 780 confocal microscope (Zeiss) after staining with propidium iodide (Invitrogen).

2.4 | IAA metabolite profiling

For each M_3 candidate mutant line, five biological replicates containing ~10 mg (FW) of 7-day-old seedlings were harvested. The control parental lines were represented by 15–20 replicates from different plates so that variability caused by the position of the plates is buffered in reference data. Extraction, purification, and quantification of targeted compounds (Ant, Trp, IPyA, IAOx, IAN, IAA, oxIAA, IAA-Asp, IAA-Glu, IAA-glc, and oxIAA-glc) were performed according to Pěňčík et al. (2018). Briefly, samples were extracted in 1 mL of cold 50 mmol/L phosphate buffer (pH 7.0) containing 0.1% sodium diethyldithiocarbamate and a mixture of isotope-labelled internal standards. A 200 μ L portion of the extract was acidified to pH 2.7 with HCl and purified using in-tip micro solid phase extraction (in-tip μ SPE). Another 200 μ L portion of the extract was derivatized with cysteamine, acidified to pH 2.7 with HCl, and purified using in-tip μ SPE. Eluted samples were evaporated under reduced pressure, reconstituted in 10% aqueous methanol, and analysed using an ultra-high performance liquid chromatograph I-Class (Waters) equipped with a Kinetex C18 column (50 mm x 2.1 mm, 1.7 μ m; Phenomenex) and coupled with tandem mass spectrometer Xevo TQ-XS (Waters).

2.5 | Data analysis

Multivariate data analysis was conducted using ‘Soft Independent Modelling of Class Analogies’ (SIMCA) software version 13 (Umetrics AB). Since none of the $DR5_{pro}$:VENUS samples reached detectable levels of IAOx, the PCAs for drX lines were obtained based on the other ten metabolites.

2.6 | Mapping-by-sequencing

We followed different mapping-by-sequencing approaches to identify the genes affected in *dii365.3* and *dii571.1*. For *dii365.3*, we generated a mapping population from the backcross to the $35S_{pro}$:*DII*-VENUS parental line. Then, we sequenced the F_2 mutant population and the parental line. For *dii571.1*, we also generated an F_2 mapping population by backcrossing to the parental line, but in this case, we sequenced two mapping populations: one showing wild-type phenotype and one showing mutant phenotype. Between 5–20 μ g of nuclear DNA was isolated from 1 g of seedlings from each population using a previously described method (Hanania et al. 2004). Whole genome sequencing was carried out at BGI Hong Kong using a BGISEQ-500 sequencing platform. Sequencing statistics are detailed in Table S2. Trimmed FASQ files were used to map the causative

mutations using the graphical interface-containing software (for Linux) EASYMAP (Lup et al. 2021), using default parameters. Once EASYMAP defined the candidate intervals (shown in Figures 2K and 3F), candidate mutations were manually analysed. Raw reads were deposited in the short read archive (SRA) under the references SAMN15549721 (parental $35S$:*DII*-VENUS), SAMN15549723 (F_2 mutant population for *dii365.3*), SAMN15549724 (F_2 wild type population for *dii571.1*), and SAMN15549725 (F_2 mutant population for *dii571.1*).

2.7 | Accession numbers

CYP83A1 (At4g13770), MIAO (At3g54660), SUR2 (At4g31500).

3 | RESULTS

To find mutants affected in IAA metabolism or homeostasis, we designed a forward genetic screen with multiple filtering steps (Figure 1A). For being able to monitor *in vivo* the status of the auxin signalling, we mutagenized with ethyl methanesulfonate (EMS) seeds (M_0) from two of the most commonly used auxin fluorescent reporters $DR5_{pro}$:VENUS (Heisler et al. 2005), and $35S_{pro}$:*DII*-VENUS (Brunoud et al. 2012). We allowed the M_1 plants to self-pollinate and screened 2230 M_2 families looking for at least one of the following features: (1) morphological phenotype, and/or (2) aberrant reporter signal. We found a few aberrant patterns for fluorescent signal, including patterns compatible with higher and lower IAA levels (Figure 1B). Morphologically, the variety was greater, ranging from pale leaves, shorter roots, loss of apical dominance, more branched root system, spontaneous formation of adventitious roots, hairy roots or etiolated seedlings (Figure 1C). This first double pre-screen allowed us to filter out more than 80% of M_2 plants, keeping 325 M_3 lines whose Mendelian transmission of the selected phenotype was confirmed in the M_4 generation.

These 325 selected candidates were then subjected to high-throughput quantification of IAA and ten related metabolites: Ant, Trp, IAOx, IAN, IPyA, IAA-glc, oxIAA-glc, oxIAA, IAA-Glu, and IAA-Asp (Pěňčík et al. 2018). Five biological replicates of each candidate and fifteen to thirty-eight replicates of the corresponding parental line were analysed, totalizing 1678 auxin metabolite profiles (Table S3). In order to digest this amount of data, we applied multivariate data analysis (MVDA) to uncover lines with altered IAA-metabolite profiles, which potentially carry mutations that directly disturb IAA metabolism (Figure 1D–I). MVDA allowed us to point to several lines showing great separation from parental lines. From the $35S_{pro}$:*DII*-VENUS (*diiX* mutants), a clear separation from the model was observed for *dii830.1*, *dii192.1*, *dii365.3*, *dii766.2* or *dii571.1* among others (Figure 1D,E) while for lines derived from mutagenizing $DR5_{pro}$:VENUS (*drX* mutants), *dr693*, *dr606*, *dr549*, *dr577.2* or *dr263.1* showed an explicit differential behaviour from the model (Figure 1G,H). To confirm that this methodology can pinpoint mutants with an altered IAA metabolism or homeostasis, we selected three candidate lines

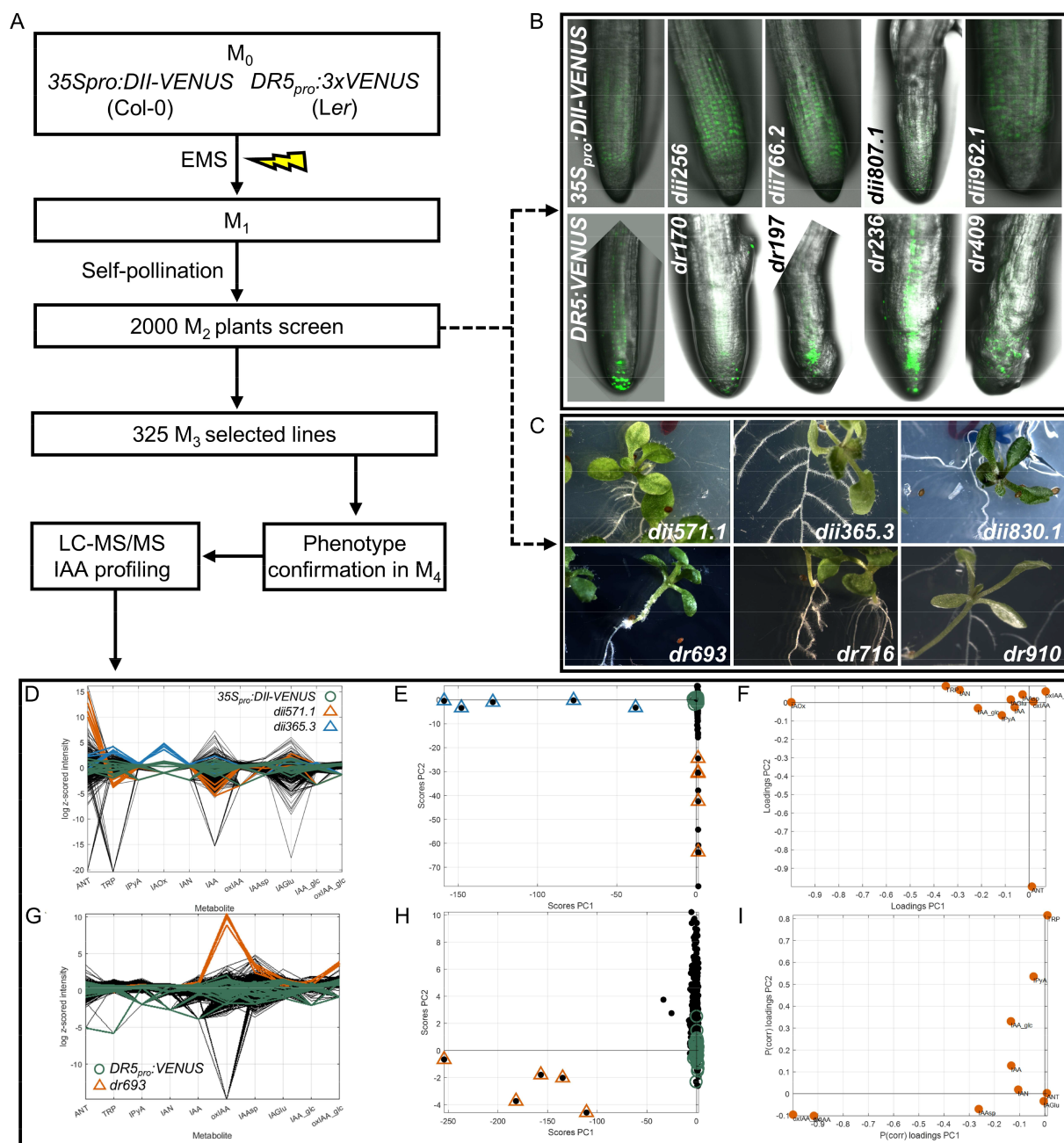


FIGURE 1 Genetic screen design to find IAA metabolism mutants. (A) Workflow of the screening strategy. Seeds from the auxin reporters *35S_{pro}:DII-VENUS* and *DR5:VENUS* were mutagenized with EMS. M_1 plants were self-pollinated, and M_2 generation was screened for fluorescent aberrant patterns (B) or morphological phenotypes (C). (D–I) Multivariate Data Analyses was performed on the screened lines. (D, G) Profiles for each sample and all variables used in the PCA. Since none of the *DR5_{pro}:VENUS* samples reach detectable levels of IAA_{ox}, the PCAs for *drX* lines were obtained based on the other ten metabolites. Values were log-transformed, subtracted from the average and divided by the standard deviation of (D) *35S_{pro}:DII-VENUS* and (G) *DR5:VENUS*. Only data from lines subjected to further validation was coloured. (E, H) PCA scores (E, H) and loading scores (F, I). Data was subtracted from the average and divided by the standard deviation of (E, F) *35S_{pro}:DII-VENUS* and (H, I) *DR5:VENUS*.

showing the greatest separation from the corresponding model and an easy-to-assign morphological phenotype for further characterization: *dii571.1*, *dii365.3*, and *dr693* (Figure 1D–I).

The phenotype of the *dii571.1* mutant, with some variable expressivity, consists of short roots and a certain loss of apical dominance (Figure 2A–D). *DII-VENUS* signal is enhanced in *dii571.1* roots,

suggesting lower IAA levels than the parental line, a feature confirmed by our IAA metabolite screen data, which also revealed high levels of Ant in this mutant (Figures 1D,E and 2E–G; Table S3). To identify the *dii571.1* mutation, the mutant was backcrossed to the parental line to generate an F_2 mapping population. We harvested two pools of plants, one comprising 146 phenotypically wild-type plants and

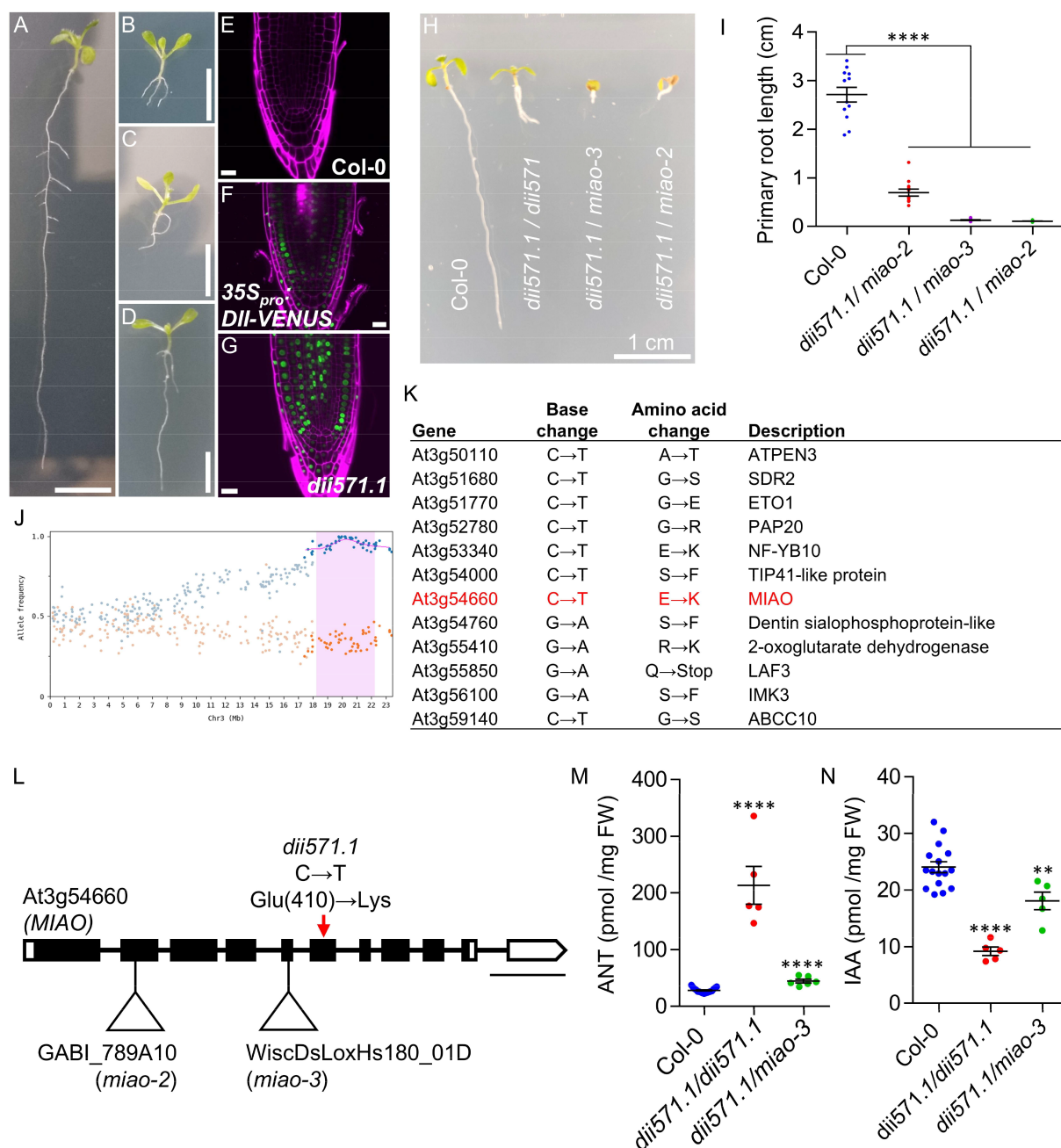


FIGURE 2 The *dii571.1* is a new allele of the *MIAO* gene and affects IAA homeostasis. (A–D) Phenotype of 10-day-old vertically grown seedlings of (A) the parental *35S_{pro}:DII-VENUS*, (B–D) *dii571.1*; *35S_{pro}:DII-VENUS*. (E–G) Confocal micrographs detecting the VENUS signal over root tips stained with propidium iodide of (E) non-transgenic Col-0, (F) *35S_{pro}:DII-VENUS* and *dii571.1*; *35S_{pro}:DII-VENUS*. (H, I) Primary root length pictures (H) and quantification (I) of the wild-type Col-0, the homozygous *dii571.1*, and the heterozygous *dii571.1/miao-3*, and *dii571.1/miao-2* plants. (J) Easymap output of SNPs allelic frequency visualization at chromosome 3. Blue and orange dots correspond to F₂ mutant, and wild-type populations, respectively. (K) Candidate mutation list present within the region shaded in magenta in (J). (L) Architecture of the *MIAO* gene and illustration of the nature and location of the mutations studied in this work. Boxes indicate exons and lines introns. White boxes represent untranslated regions. Triangles represent T-DNA insertions (*miao-2* and *miao-3*); the red arrow points to the EMS-induced C-to-T transition, which changes the Glu410 for a Lys. (M, N) Ant (M) and IAA (N) quantification in picomoles per mg of fresh tissue was performed for the different allelic combinations. Asterisks indicate values significantly different from the Col-0 in a Student's *t*-test [$** p < 0.01$; $**** p < 0.0001$; (I) $12 \leq n \leq 19$, (M) $5 \leq n \leq 17$, (N) $12 \leq n \leq 18$]. Scale bars indicate (A–D) 0.5 cm, (E–G) 20 μ m, (H) 1 cm, and (L) 0.5 kb.

another containing 114 phenotypically mutant plants. Nuclear DNA was purified from mapping populations and subjected to whole-genome sequencing with a high sequencing depth, ranging from 111x

to 129x (Table S2). We then used the mapping software Easymap to find candidate mutations (Lup et al. 2021). The analysis of the allelic frequency of both populations clearly defined a candidate interval in

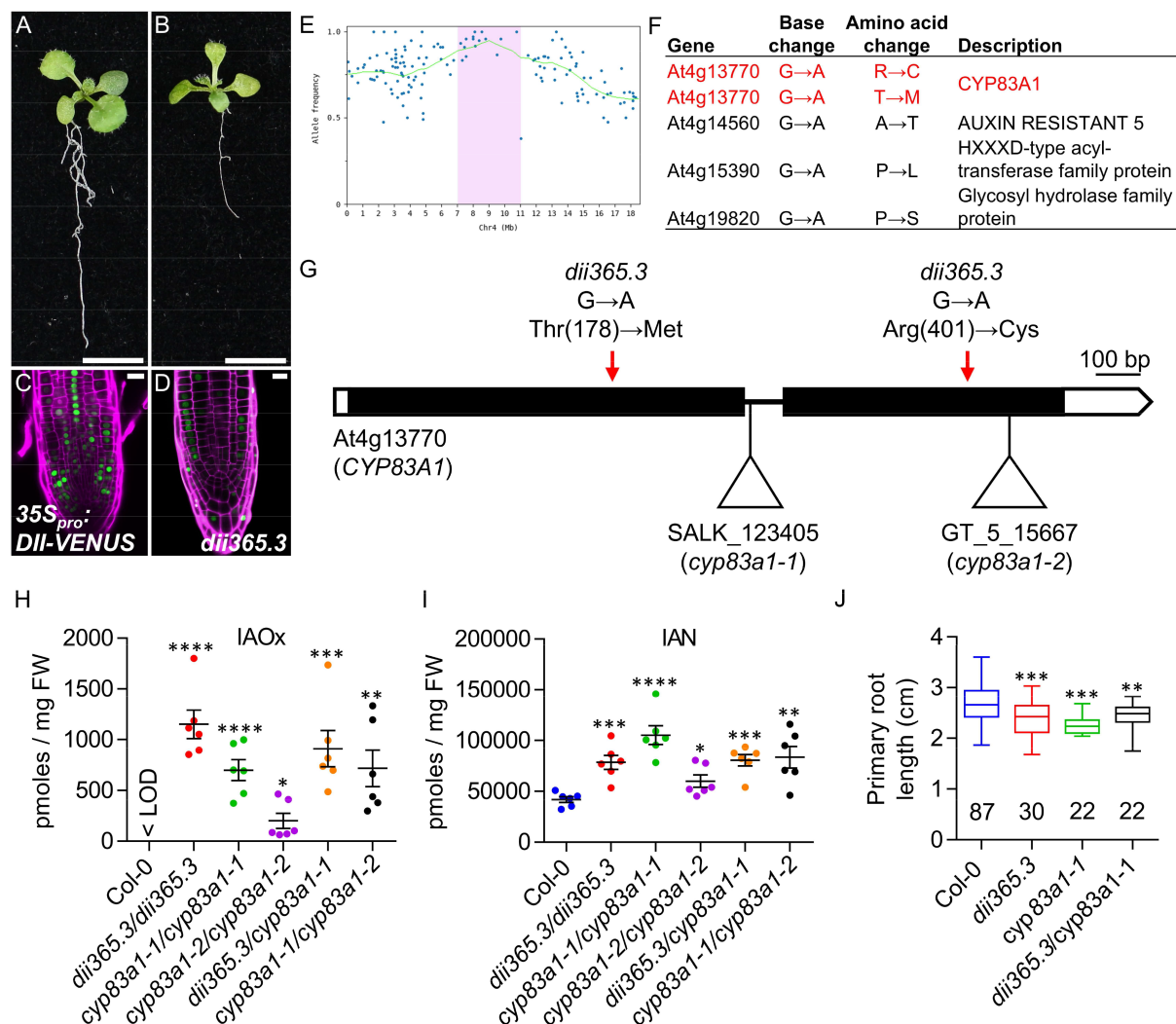


FIGURE 3 The *dii365.3* mutant carries two mutations in CYP83A1. (A, B) Phenotype of 10-day-old vertically grown seedlings of (A) the parental *35S_{pro}:DII-VENUS*, and (B) *dii365.3*. (C, D) Confocal micrographs detecting the VENUS signal over root tips stained with propidium iodide of (C) *35S_{pro}:DII-VENUS* and (D) *dii365.3*; *35S_{pro}:DII-VENUS*. (E) EasyMap output of SNPs allelic frequency visualization of the F₂ mutant population at chromosome 4. (F) Candidate mutation list present within the region shaded in magenta in (E). (G) Architecture of the CYP83A1 gene with illustration of the nature and location of the mutations studied in this work, following the pattern shown in Figure 2. (H, I) IAOx (H) and IAN (I) quantification in picomoles per mg of fresh tissue was performed for the different allelic combinations. (J) Primary root length was determined for the assorted genotypes. Asterisks indicate values significantly different from the Col-0 in a Student's *t*-test [$* p < 0.05$; $** p < 0.01$; $*** p < 0.001$; $**** p < 0.0001$; (H, I) $n = 6$, (J) $22 \leq n \leq 87$]. Numbers above the X-axis of (J) indicate the number of roots analysed per genotype. Scale bars indicate (A, B) 5 mm, (C, D) 20 μ m, and (G) 100 bp.

chromosome 3 (Figure 2J). Several potential mutations were found within the interval (Figure 2K). Among them, one stood up as a very good candidate: a C-to-T transition in the gene At3g54660, which introduces a non-synonymous substitution of glutamine for a lysine residue in position 410 (Gln410-to-Lys). This gene encodes a plastid-localized Glutathione Reductase, whose role in auxin homeostasis was previously reported (Yu et al. 2013). Null alleles of this gene, coined MIAO, manifest embryo-lethality (Tzafrir et al. 2004). We obtained two publicly available T-DNA lines: GABI_789A10 and WiscD-LoxHs180_01D, which we refer to hereafter as *miao-2* and *miao-3* (Figure 2L). As expected, we could not find homozygous plants for such insertions, but we identified phenotypically wild-type

heterozygous plants for these alleles. We then crossed our *dii571.1* line to the heterozygous T-DNA insertional lines, finding a 1:1 segregation of wild-type plants and plants showing severe root inhibition growth (40 wild type:37 mutant; Figure 2H). Quantification of both the primary root length and the levels of Ant and IAA in *dii571.1* and F₁ plants confirmed their allelism and, therefore, identified *dii571.1* as a new allele of the MIAO gene (Figure 2I,M,N).

One uncommon feature for most of the screened lines was to show detectable levels of IAOx (Table S3). Indeed, only three lines (*dii365.3*, *dr606.1*, and *dr693*) showed detectable and remarkably higher levels of IAOx than their corresponding controls. Since *dii365.3* and *dr693* also showed a great separation from the model (Figure 1D,

(E,G,H), we decided to select them for further analyses. Plants carrying the *dii365.3* mutation present shorter roots than the wild-type and decreased DII-VENUS signal at the root tip, suggesting an accumulation of IAA (Figure 3A-D). To identify the mutated gene in the *dii365.3* line, we carried out a similar strategy as for *dii571.1*. We first backcrossed *dii365.3* plants to the parental line to generate a mapping population. We harvested 35 phenotypically mutant plants and sequenced the nuclear DNA of the mapping population, which was compared to the parental line 35_{pro}:DII-VENUS. Parental and mapping populations were sequenced to 56x and 36x genome depths, respectively, allowing us to narrow down a candidate interval in chromosome 4 (Figure 3E). The list of candidate mutations within the interval contained just a few genes with changes in coding regions (Figure 3F). Among them, we found that At4g13770 carried two G-to-A transitions, generating two amino acid changes, Thr178-to-Met, and Arg401-to-Cys, in the CYTOCHROME P450 enzyme 83A1 (CYP83A1). We obtained two publicly available *cyp83a1* lines carrying a T-DNA insertion in the first intron (SALK_123405; hereafter *cyp83a1-1*) and a transposon in the second exon (GT_5_15667; *cyp83a1-2*) of the CYP83A1 gene. IAA metabolite profiling revealed

high levels of IAOx and IAN in seedlings from homozygous and heterozygous mutant plants (Figures 3H,I and S1). Moreover, the reduction in *dii365.3* primary root length was not complemented in *dii365.3/cyp83a1-1* heterozygous plants, together confirming their allelism (Figure 3J) and demonstrating that *DII365.3* is CYP83A1.

When analysing the phenotype of *dr693* plants, we realized that it spontaneously generated adventitious roots in the hypocotyl (Figure 4A,B), a relatively rare phenomenon (Lakehal et al. 2019). While preparing the backcrossing families to map the mutations, we tested its potential allelism with the well-characterized mutant *super-root-2-1* (*sur2-1*) (Barlier et al. 2000), which shows this spontaneous organogenesis. We then vertically grew both mutants, *dr693* and *sur2-1*, and the F₁ family for 1 day in the light, transferred them to darkness for three days to promote hypocotyl elongation and placed them back to light for ten additional days. In contrast to the parental *DR5_{pro}:VENUS* line, *dr693* and *sur2-1* mutants and the heterozygous plants showed spontaneous formation of adventitious roots, strongly indicating their allelism. We then sequenced the *SUR2* gene in *dr693* plants and found a C-to-T transition that generates a premature stop

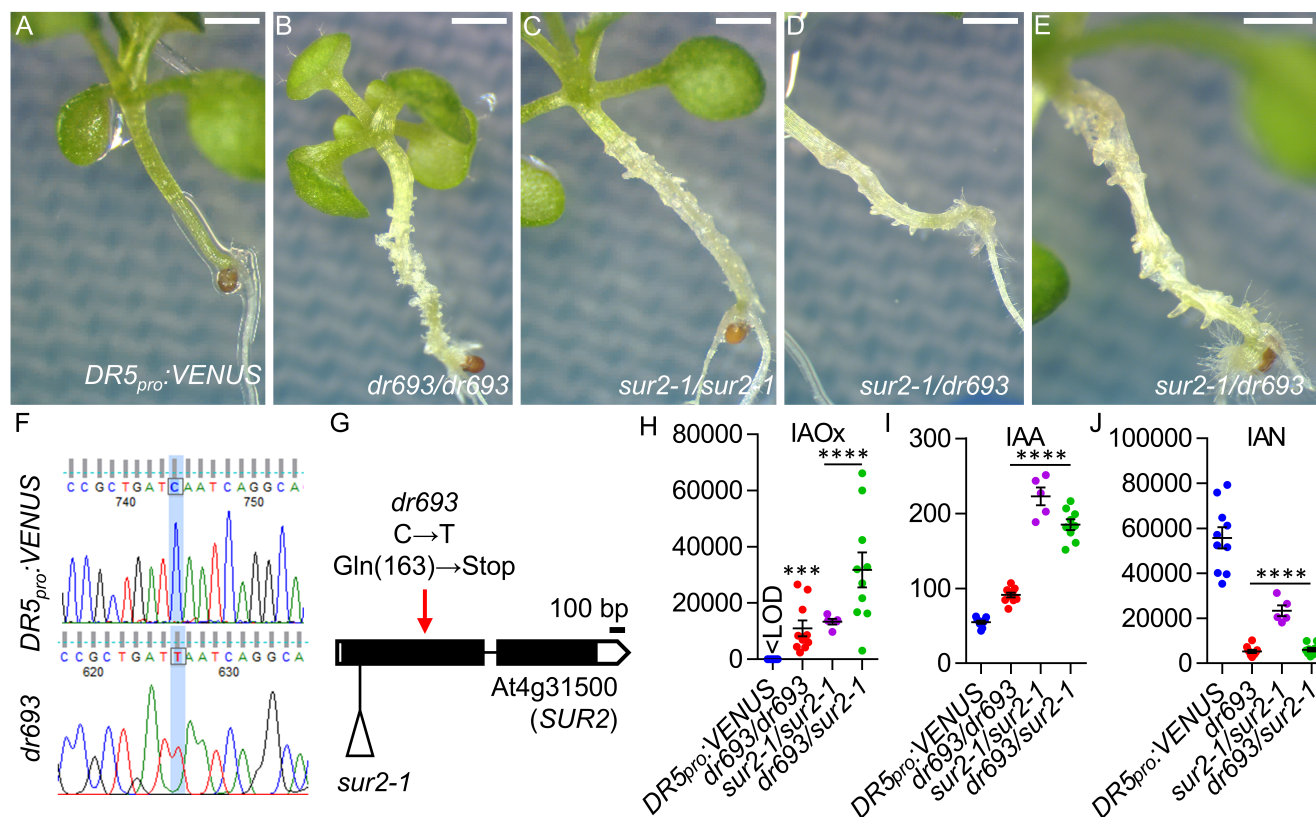


FIGURE 4 The phenotype of *dr693* is due to a mutation in *SUR2*. (A-E) Phenotype of 14-day-old vertically grown seedlings kept in darkness for three days of (A) the parental *DR5_{pro}:VENUS*, (B, C) homozygous (B) *dr693* and (C) *sur2-1*, and heterozygous (D, E) *dr693/sur2-1*. (F) Electropherogram of the *SUR2* region where the mutation was found in *dr693*, with the highlighted C-to-T transition. (G) Architecture of the *SUR2* gene with illustration of the nature and location of the mutations studied in this work, following the pattern shown in Figure 2. (H-J) Quantification, in picomoles per mg of fresh weight, of the levels of (H) IAOx, (I) IAA, and (J) IAN in the assorted genotypes. Asterisks indicate levels significantly different from those in *DR5_{pro}:VENUS* in a Student's t-test [*** $p < 0.001$; **** $p < 0.0001$; (H-J) $5 \leq n \leq 10$]. Scale bars indicate (A-E) 1 mm, and (G) 100 bp.

codon in the Gln163 (Figure 4F,G). Finally, both the parental and the F_1 family (Figure 4H-J; Figure S2) were subjected to IAA metabolite profiling, all in all confirming that this mutation in *SUR2* causes the phenotype of *dr693*.

4 | DISCUSSION

Our pilot screen results demonstrate that coupling high-throughput metabolite profiling to an EMS-based screening is a suitable approach to finding mutants affected in a process of interest. While forward genetic screens bear as intrinsic limitation, their inability to overcome gene redundancy, a common feature of enzyme families as some of the ones involved in IAA homeostasis (Mateo-Bonmatí et al. 2021, Casanova-Sáez et al. 2022), these approaches are ideal for isolating weak alleles of essential genes and do not rely on previous knowledge on the genes of interest.

The present work identified a viable allele of the *MIAO* gene, encoding an essential glutathione reductase. The study of single and multiple mutants affecting the redox regulation has revealed a functional connection with auxin transport and metabolism since they phenocopied typical mutant traits of auxin-deficient mutants such as impaired root growth, reduced formation of lateral organs, loss of apical dominance, or defects in the vasculature (Bashandy et al. 2011, Yu et al. 2013). Our *dii571.1* mutant further supports a link between glutathione and auxin homeostasis, which will require detailed investigation.

Metabolic pathways are often interconnected by sharing common intermediate metabolites. In the case of IAA, the best-documented connection, albeit specific to *Brassicaceae*, is with the route of the indole glucosinolates (GLS), a group of defence molecules that are hydrolysed in response to infection, resulting in toxic compounds to many pathogens and herbivores (Malka and Cheng 2017). IAOx is the common node for both IAA and GLS pathways. While IAOx can be converted to IAN and subsequently to IAA by action of CYP71A13 and CYP71B15 (Casanova-Sáez et al. 2021), IAOx is also the substrate for the production of aromatic GLS (Bak and Feyereisen 2001, Hemm et al. 2003, Gigolashvili et al. 2007). *SUR2*/CYP83B1 catalyses the conversion of the Trp-derived IAOx to *s*-alkylthiohydroximate, while CYP83A1 acts on the conversion of aliphatic oximes derived from methionine, although it can also use IAOx as substrate with lower affinity compared to *SUR2* (Naur et al. 2003). Interestingly, our results showed that both IAOx and IAN are highly accumulated in CYP83A1-deficient *dii365.3* mutants, which suggests a stronger connection than previously thought between the aliphatic GLS synthesis and the IAA metabolic pathway.

The identification of the remaining lines from the current screen or similar future screens will be crucial in bridging gaps in our understanding of IAA metabolic pathways, like the proposed Trp-independent pathway for IAA biosynthesis (Nonhebel 2015), the genes involved in the conversion of IAN and of IAM to IAA, and, ultimately, how these pathways integrate with various stress response mechanisms.

AUTHOR CONTRIBUTIONS

R. C.-S., A.P., R. M.-V., O.N., K.L. and E.M.-B. designed the methodology. R.C.-S., R.M.-V., and F.B. performed the EMS screening. R.C.-S. and R.P. performed the statistical analyses and candidate selection. A.P., and O.N. performed the metabolic profiling. R.C.-S. and E.M.-B. generated the mapping population, and mutant characterization. O.N., K.L. and E.M.-B. obtained funding and provided resources. E.M.-B. prepared the original draft. All authors reviewed and edited the manuscript.

ACKNOWLEDGEMENTS

We thank NASC for providing the plant lines used in this work and Roger Granbom (UPSC, Umeå) and Andrea Novotná (LGR, Olomouc) for their technical assistance. We also acknowledge the Swedish Metabolomics Centre and the UPSC Microscopy Facility.

FUNDING INFORMATION

The Knut and Alice Wallenberg Foundation (KAW 2016.0352); the Carl Tryggers foundation (CTS 12:289 and CTS 13:275); the Swedish Research Council (2014-04514); Kempeförfattelserna (JCK-1811, JCK-1111); Grant RYC2021-030895-I funded by MICIU/AEI/10.13039/501100011033 and by European Union NextGenerationEU/PRTR; Grant PID2023-147737NA-I00 funded by MICIU/AEI/10.13039/501100011033 and “ERDF/EU”; Internal Grant Agency of Palacký University Olomouc IGA_PrF_2024_013.

DATA AVAILABILITY STATEMENT

All data generated or analysed during this study are provided in this published article and its supplementary data files or will be provided upon reasonable request.

ORCID

Rubén Casanova-Sáez  <https://orcid.org/0000-0001-5683-7051>
 Aleš Pěňčík  <https://orcid.org/0000-0002-1314-2249>
 Rafael Muñoz-Viana  <https://orcid.org/0000-0002-1363-6978>
 Federica Brunoni  <https://orcid.org/0000-0003-1497-9419>
 Rui Pinto  <https://orcid.org/0000-0002-8527-4873>
 Ondřej Novák  <https://orcid.org/0000-0003-3452-0154>
 Karin Ljung  <https://orcid.org/0000-0003-2901-189X>
 Eduardo Mateo-Bonmatí  <https://orcid.org/0000-0002-2364-5173>

REFERENCES

- Bak S, Feyereisen R (2001) The involvement of two p450 enzymes, CYP83B1 and CYP83A1, in auxin homeostasis and glucosinolate biosynthesis. *Plant Physiol* 127(1): 108–118
- Barlier I, Kowalczyk M, Marchant A, Ljung K, Bhalerao R, Bennett M, Sandberg G, Bellini C (2000) The *SUR2* gene of *Arabidopsis thaliana* encodes the cytochrome P450 CYP83B1, a modulator of auxin homeostasis. *Proc Natl Acad Sci U S A* 97(26): 14819–14824
- Bashandy T, Meyer Y, Reichheld JP (2011) Redox regulation of auxin signaling and plant development in *Arabidopsis*. *Plant Signal Behav* 6(1): 117–119
- Brunoud G, Wells DM, Oliva M, Larrieu A, Mirabet V, Burrow AH, Beeckman T, Kepinski S, Traas J, Bennett MJ, Vernoux T (2012) A

- novel sensor to map auxin response and distribution at high spatio-temporal resolution. *Nature* 482(7383): 103–106
- Casanova-Sáez R, Voß U (2019) Auxin Metabolism Controls Developmental Decisions in Land Plants. *Trends Plant Sci* 24(8): 741–754
- Casanova-Sáez R, Mateo-Bonmatí E, Ljung K (2021) Auxin Metabolism in Plants. *Cold Spring Harb Perspect Biol* 13(3)
- Casanova-Sáez R, Mateo-Bonmatí E, Šimura J, Pěňčík A, Novák O, Staswick P, Ljung K (2022) Inactivation of the entire Arabidopsis group II GH3s confers tolerance to salinity and water deficit. *New Phytol* 235(1): 263–275
- Gigolashvili T, Berger B, Mock HP, Muller C, Weissshaar B, Flugge UI (2007) The transcription factor HIG1/MYB51 regulates indolic glucosinolate biosynthesis in Arabidopsis thaliana. *Plant J* 50(5): 886–901
- Hanania U, Velcheva M, Sahar N, Perl A (2004) An improved method for isolating high-quality DNA from *Vitis vinifera* nuclei. *Plant Mol Biol Rep* 22: 173–177
- Heisler MG, Ohno C, Das P, Sieber P, Reddy GV, Long JA, Meyerowitz EM (2005) Patterns of auxin transport and gene expression during primordium development revealed by live imaging of the Arabidopsis inflorescence meristem. *Curr Biol* 15(21): 1899–1911
- Hemm MR, Ruegger MO, Chapple C (2003) The Arabidopsis ref2 mutant is defective in the gene encoding CYP83A1 and shows both phenylpropanoid and glucosinolate phenotypes. *Plant Cell* 15(1): 179–194
- Jing H, Wilkinson EG, Sageman-Furnas K, Strader LC (2023) Auxin and abiotic stress responses. *J Exp Bot* 74(22): 7000–7014
- Kazan K, Manners JM (2009) Linking development to defense: auxin in plant-pathogen interactions. *Trends Plant Sci* 14(7): 373–382
- Lakehal A, Dob A, Novák O, Bellini C (2019) A DAO1-Mediated Circuit Controls Auxin and Jasmonate Crosstalk Robustness during Adventitious Root Initiation in Arabidopsis. *Int J Mol Sci* 20(18)
- Lup SD, Wilson-Sánchez D, Andreu-Sánchez S, Micol JL (2021) Easy-map: A User-Friendly Software Package for Rapid Mapping-by-Sequencing of Point Mutations and Large Insertions. *Front Plant Sci* 12: 655286
- Malka SK, Cheng Y (2017) Possible Interactions between the Biosynthetic Pathways of Indole Glucosinolate and Auxin. *Front Plant Sci* 8: 2131
- Mateo-Bonmatí E, Casanova-Sáez R, Šimura J, Ljung K (2021) Broadening the roles of UDP-glycosyltransferases in auxin homeostasis and plant development. *New Phytol* 232(2): 642–654
- Naur P, Petersen BL, Mikkelsen MD, Bak S, Rasmussen H, Olsen CE, Halkier BA (2003) CYP83A1 and CYP83B1, two nonredundant cytochrome P450 enzymes metabolizing oximes in the biosynthesis of glucosinolates in Arabidopsis. *Plant Physiol* 133(1): 63–72
- Nonhebel HM (2015) Tryptophan-Independent Indole-3-Acetic Acid Synthesis: Critical Evaluation of the Evidence. *Plant Physiol* 169(2): 1001–1005
- Pěňčík A, Casanova-Sáez R, Pilařova V, Žukauskaitė A, Pinto R, Micol JL, Ljung K, Novák O (2018) Ultra-rapid auxin metabolite profiling for high-throughput mutant screening in Arabidopsis. *J Exp Bot* 69(10): 2569–2579
- Tzafrir I, Pena-Muralla R, Dickerman A, Berg M, Rogers R, Hutchens S, Sweeney TC, McElver J, Aux G, Patton D, Meinke D (2004) Identification of genes required for embryo development in Arabidopsis. *Plant Physiol* 135(3): 1206–1220
- Yu X, Pasternak T, Eiblmeier M, Ditengou F, Kochersperger P, Sun J, Wang H, Rennenberg H, Teale W, Paponov I, Zhou W, Li C, Li X, Palme K (2013) Plastid-localized glutathione reductase2-regulated glutathione redox status is essential for Arabidopsis root apical meristem maintenance. *Plant Cell* 25(11): 4451–4468

SUPPORTING INFORMATION

Additional supporting information can be found online in the Supporting Information section at the end of this article.

How to cite this article: Casanova-Sáez, R., Pěňčík, A., Muñoz-Viana, R., Brunoni, F., Pinto, R., Novák, O. et al. (2025) A suitable strategy to find IAA metabolism mutants. *Physiologia Plantarum*, 177(2), e70166. Available from: <https://doi.org/10.1111/ppl.70166>